Table 1: Molar Proportions of Reactants in MCH Experiments

Mix #	ϕ	MCH	O_2	N_2	Ar
1	1.0	1	10.5	12.25	71.75
2	0.5	1	21.0	0.00	73.50
3	1.5	1	7.0	16.35	71.15

1 Procedures

The liquid fuel (methyl-cyclohexane, 99.0% purity) is massed to a precision of 0.01 g in a syringe before being injected into the mixing tank through a septum. The proportions of oxygen (99.9999% purity), nitrogen (99.9995% purity), and argon (99.9999% purity) are determined by specifying the oxidizer composition, the equivalence ratio, and the total mass of fuel. The gases are added to the mixing tank manometrically at room temperature.

Three different mixtures of MCH/O_2/N_2/Ar are prepared in this study, as outlined in Table 1. These mixtures (denoted as Mix #1–3) match the mixtures prepared in our previous work with MCH in the RCM [16]. The equivalence ratios corresponding to Mix #1–3 are $\phi = 1.0, 0.5,$ and 1.5, respectively. As in the previous RCM experiments, the mole fraction of MCH is held constant and the mole fraction of O2 is varied to adjust the equivalence ratio. This experimental design allows these data to be used to validate chemical kinetic models for changes in O2 concentration, which is an important variable in internal combustion engines where exhaust gas recirculation is used to reduce the oxygen concentrations to avoid NOx formation. Few validation data for ignition are available for changing oxygen concentrations. In addition, the relative proportions of O2, N2, and Ar are adjusted so that the same specific heat ratio is maintained in the three mixtures. The utility of this experimental design will be discussed in due course.

2 Model Improvements

Through collaboration with researchers at Lawrence Livermore National Laboratories, many improvements to the chemical kinetic model for MCH were made. Some of the major improvements

are highlighted below; see the article for more detail. It should be noted that the improvement relative to the model from 2007 by Pitz et al. [1] is substantial.

1. The base C_1-C_4 chemistry has been updated with the AramcoMech version 1.3 [2]

2. The aromatics base chemistry was updated with the latest LLNL-NUIG model [3]

3. The cyclohexane sub-model was updated with a new version from Silke et al. [4]

4. Rates of abstraction reactions from MCH have been updated with recently measured experimental values [5] and standardized according to the LLNL reaction rate rules [6]

5. Products of MCH breakdown with unsaturated rings such as methylcyclohexene were previously lumped into one species for simplicity. In the new model, they have been unlumped and provide improved fidelity in modeling these species. [7]

6. The reaction rates of some low-temperature specific reactions were updated using new quantum chemical calculations to compute the rate. Other reaction rates were updated from similar calculations performed by Fernandes et al. [8]

7. The activation energy of the ketohydroperoxide decomposition reactions was increased to bring it into closer agreement with the activation energy used by Metcalfe et al. [2]. This change has a dramatic effect on the low-temperature ignition delays, as shown in Sec. 4.

3   Experimental Results

The experimental ignition delays measured at the three equivalence ratios and compressed pressure of 50 bar are shown in Fig. 1. The open symbols are the overall ignition delays and the filled symbols are the first stage ignition delays. The vertical error bars on the experimental data represent twice the standard deviation of all of the experiments at that condition. Detailed uncertainty analysis of the deduced compressed temperature was conducted in **??** where the maximum uncertainty of the compressed temperature was found to be approximately ±1%.

The negative temperature coefficient (NTC) region is an important feature of low temperature ignition where the ignition delay time increases with increasing temperature. The NTC region of the overall ignition delay is evident in Fig. 1 for the $\phi = 1.5$ case (Mix #3) and approximately includes the temperature range of $T_C = 775$–840 K. For $\phi = 1.5$, first stage ignition is evident for conditions in the range of $T_C = 740$–800 K.

For $\phi = 1.0$ (Mix #1), the NTC region of the overall ignition delay could not be completely resolved. Only three conditions in the low temperature region and three conditions in the high temperature region are shown in Fig. 1. The experimental pressure traces during the compression stroke for intermediate temperature conditions were seen to deviate from their non-reactive counterparts, demonstrating appreciable reactivity therein. Hence, those data are not included in 1.

For the experiments at $\phi = 0.5$ (Mix #2), only three data points in the low temperature region are reported and none of them exhibits two-stage ignition response. As the temperature is increased further, noticeable reactivity during the compression stroke is evident.

As stated earlier, the mole fraction of MCH is held constant in this study, while the mole fraction of the oxidizer is changed to modify the equivalence ratio. Figure 1 demonstrates that the $\phi = 0.5$ case is the most reactive (as judged by the inverse of the ignition delay) and the $\phi = 1.5$ case is the least reactive. As has been shown for other fuels, including n-butanol [9] and Jet-A [10], decreasing the equivalence ratio by increasing the oxygen mole fraction but holding the fuel mole fraction constant increases the reactivity.

4   Comparison to Model

A comparison of the experimentally measured first stage ignition delays (open symbols) and the first stage ignition delays computed using the updated model (lines) is shown in Figs. 2(a), 3(a), and 4(a) for Mix #1, #2, and #3, respectively. In addition, a comparison of the experimentally measured overall ignition delays (open symbols) and the overall ignition delay computed by the updated model (lines) is shown in Figs. 2(b), 3(b), and 4(b). The experiments include the new work
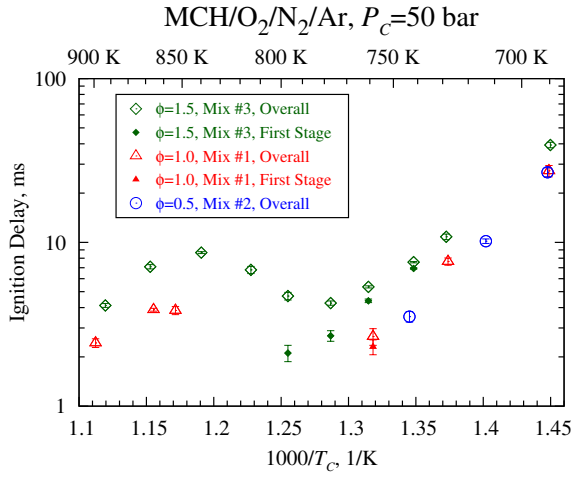
MCH/O$_2$/N$_2$/Ar, P_C=50 bar

Figure 1: Experimentally measured ignition delays at $P_C = 50$ bar for the mixture conditions in Table 1
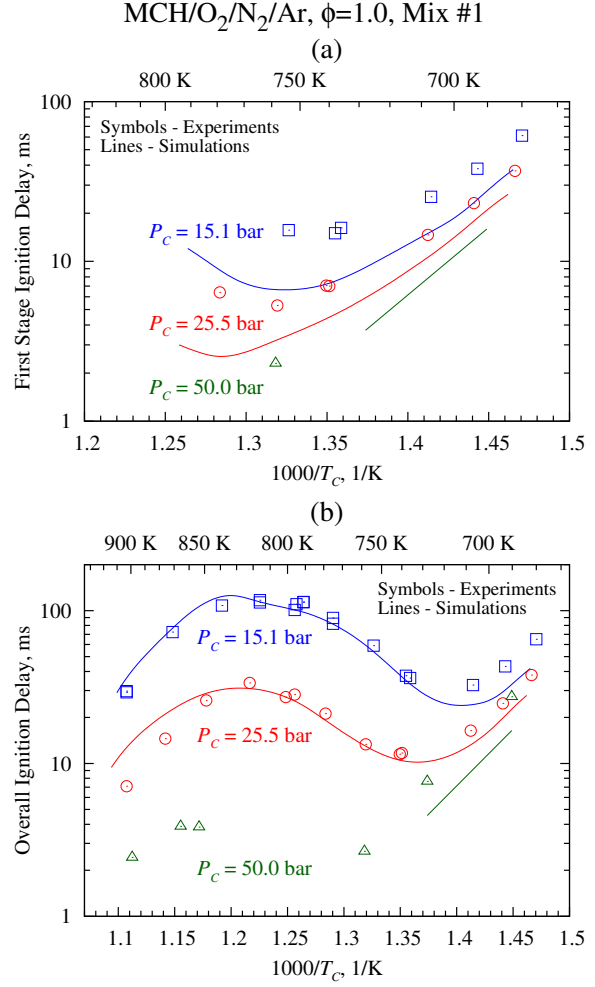
MCH/O$_2$/N$_2$/Ar, ϕ=1.0, Mix #1

Figure 2: Comparison of experimental and simulated ignition delays for three pressures for Mix #1. The data at 15.1 and 25.5 bar are from the study of Mittal and Sung [11]. (a) First stage ignition delays, (b) overall ignition delays.

being presented here at $P_C = 50$ bar in addition to the previous RCM experiments at $P_C = 15.1$ and 25.5 bar [11]. The simulations are the VPRO type of simulations. For some computational cases, substantial heat release during the compression stroke caused the computed pressure to depart from the non-reactive profile prior to EOC. Therefore, these cases are not shown in Figs. 2--3. For these conditions, the experimental pressure trace did not exhibit significant heat release during the compression stroke and the experimental pressure at EOC for the reactive case matched that of the non-reactive counterpart.

At 15.1 and 25.5 bar for Mix #1 and #2, the overall ignition delay is very well predicted for

MCH/O$_2$/N$_2$/Ar, ϕ=0.5, Mix #2

(a)

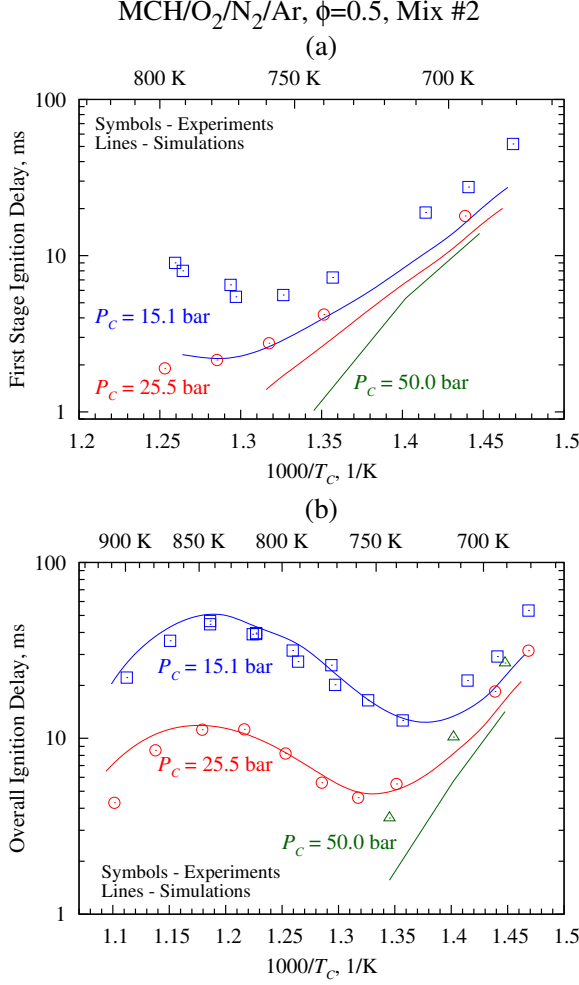MCH/O$_2$/N$_2$/Ar, ϕ=1.5, Mix #3

(a)

(b)

(b)

Figure 3: Comparison of experimental and simulated ignition delays for three pressures for Mix #2. The data at 15.1 and 25.5 bar are from the study of Mittal and Sung [11]. (a) First stage ignition delays, (b) overall ignition delays.
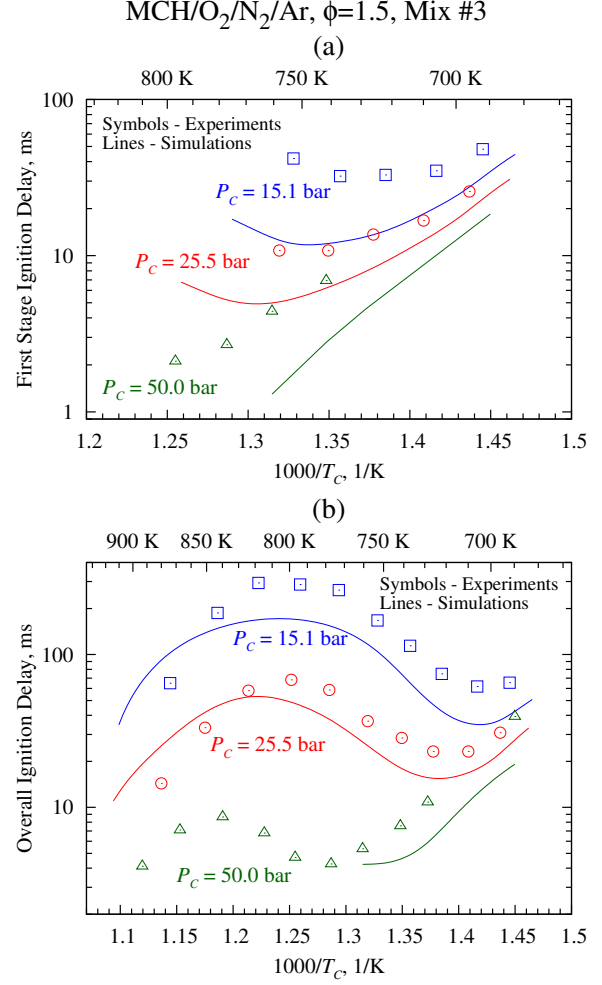
Figure 4: Comparison of experimental and simulated ignition delays for three pressures for Mix #3. The data at 15.1 and 25.5 bar are from the study of Mittal and Sung [11]. (a) First stage ignition delays, (b) overall ignition delays.

temperatures above approximately 715 K. For lower temperatures at these two equivalence ratios, the experimental ignition delays are under-predicted by the model, but the predictions are nevertheless within a factor of two of the data. For the rich case (Mix #3), the simulations under-predict the ignition delay over a wider temperature range but the results improve as temperature increases. Again, the experimental ignition delays are predicted to within approximately a factor of two. At 50 bar, the ignition delays are under-predicted for all of the equivalence ratios studied here, but the agreement is within a factor of two.

The first stage ignition delays for all of the pressure and equivalence ratios are under-predicted, but are within a factor of three of the experimental values. Furthermore, for all of the equivalence ratios tested at $P_C = 50$ bar, it is of interest to note that there are several cases where simulated ignition delays show two-stage response where the experiment shows only a single stage ignition. Nevertheless, the present mechanism is a marked improvement from the comparison performed by Mittal and Sung [11] who found that the ignition delays were strongly and uniformly over-predicted by the previous LLNL mechanism by Pitz et al. [1].

Figure 5(a)-(c) shows a comparison of selected simulated and experimentally measured pressure traces for Mix #1, #2, and #3, respectively, at $P_C = 50$ bar. Also shown in Fig. 5 is the simulated non-reactive pressure trace corresponding to each experimental condition. Small differences in the heat loss profile for different temperatures are apparent in the non-reactive pressure traces. These differences arise from the changing surface area to volume ratio of the reaction chamber at the end of compression as the compression ratio is changed to vary the compressed temperature. This highlights the importance of using VPRO simulations to compare predictions of ignition delay with the experimental data.

For Mix #1, it is clear that the simulated reactive pressure trace in Fig. 5(a) at $T_C = 866$ K (red dashed line) deviates from the non-reactive pressure trace (red dot-dot-dashed line) prior to the end of compression. The same is also true of the 797 K case shown for Mix #3 in Fig. 5(c). Remarkably, the simulated case for Mix #1 at $T_C = 866$ K predicts the overall ignition delay quite well. However, due to the heat release prior to EOC, this simulated result is not plotted in Fig. 2.
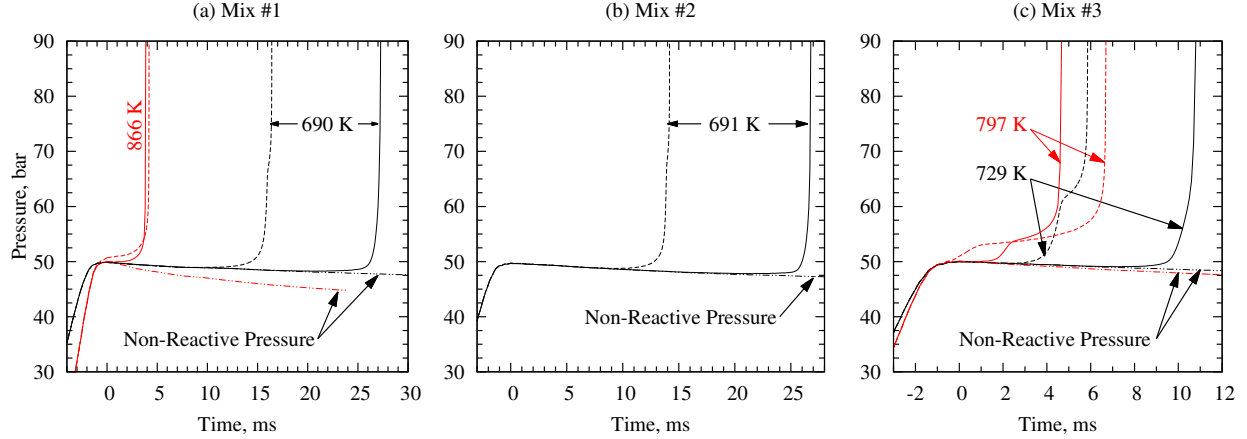
Figure 5: Comparison of selected simulated and experimental pressure traces at $P_C = 50$ bar for (a) Mix #1 (b) Mix #2 (c) Mix #3. Red lines indicate that the pressure profile of the reactive simulation deviates from the non-reactive case prior to EOC. Solid lines: experiment; dashed lines: reactive simulation; dot-dot-dashed lines: non-reactive simulation.

The simulated case for Mix #3 at $T_C = 797$ K is also not plotted on Fig. 4 due to the heat release prior to EOC; interestingly, this case under-predicts the first stage ignition delay but over-predicts the overall ignition delay. For the other simulated cases (black lines), the reactive pressure traces closely follow their non-reactive counterparts until the ignition event begins. The experimental ignition delays of these cases are under-predicted by the model. It is also seen in Fig. 5(c) for $T_C = 729$ K that the model predicts two-stage ignition, although two-stage ignition is not observed experimentally.

The current mechanism is also compared to shock tube ignition delays from the studies of Vasu et al. [12] and Vanderover and Oehlschlaeger [13]. Those studies considered the autoignition of stoichiometric mixtures of MCH with O_2/N_2 air. The comparison is shown in Fig. 6 for the near 50 atm data from those studies. Note that the experimental data shown are the raw data and are not scaled to a constant pressure, whereas the simulated ignition delays are at a constant initial pressure of 50 atm. It can be seen that the ignition delays are over-predicted over the nearly entire temperature range of 795–1160 K studied. Nevertheless, the predicted ignition delays are within approximately a factor of 1.5 of the experiments, indicating good agreement overall and a substantial improvement from the previous version of the model. Furthermore, the simulations shown here are of the CONV type and do not account for any facility dependent effects present in the experiments. Although the
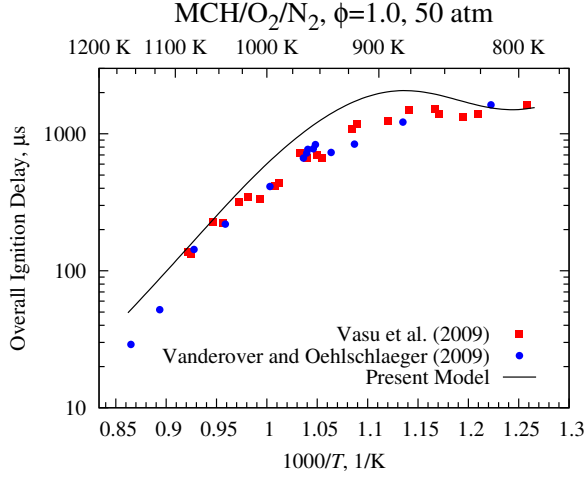
Figure 6: Comparison of the present model with the experiments from Vasu et al. [12] and Vanderover and Oehlschlaeger [13] near 50 atm and for stoichiometric mixtures in O_2/N_2 air.
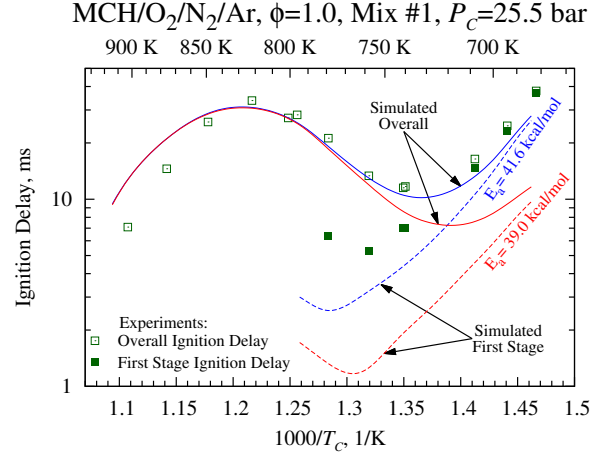

Figure 7: Comparison of mechanism performance with the activation energy of ketohydroperoxide decomposition set at 41.6 kcal/mol (blue) and 39.0 kcal/mol (red). Experimental ignition delays are shown in green symbols.

experimentalists noted in [12, 13] that the effect of such considerations is minimal in their studies, including facility dependent effects will tend to make the simulations ignite sooner and improve the agreement, especially for cases with ignition delays longer than approximately 1000 µs.

As discussed in Sec. 4, one of the updates to the model was to increase the activation energy of ketohydroperoxide decomposition, from $E_a = 39$ kcal/mol (163.2 kJ/mol) to 41.6 kcal/mol (174.1 kJ/mol). This update substantially improved the prediction of the low-temperature ignition delays, including the first stage and overall ignition delays. As mentioned by Curran et al. [14], "the high activation energy [of ketohydroperoxide decomposition] ensures an induction period during which the ketohydroperoxide concentration builds up." Furthermore, updating this activation energy does not affect the high-temperature ignition delays. A comparison of calculated ignition delays demonstrating the effect of this update is shown in Fig. 7.

5 Discussion

5.1 Path Analysis

The relatively good agreement of the updated model with the experimental data suggests that a more detailed analysis of the mechanism is a worthwhile exercise and such analysis may point the way to further improvements to the mechanism. We begin with a reaction path analysis. The present reaction path analysis is conducted using a CONV (adiabatic, constant-volume) type simulation for three initial temperatures (700 K, 800 K, and 900 K), at 25.5 bar and for Mix #1 (the stoichiometric case). For the other mixture conditions and pressures considered in this work, the absolute percentages for each channel change slightly. However, the analysis of the reaction pathways is the same for all of the equivalence ratios and pressures considered in the experiments presented previously. The three temperatures considered in this analysis correspond to the low-temperature, peak of the NTC, and high-temperature portions of the ignition delay curve illustrated in Fig. 7; their results are shown in Fig. 8 with plain text, bold text, and italic text, respectively.

The path analysis presented in Fig. 8 is an integrated analysis where the rate of production (ROP) of each species by each reaction has been integrated with respect to time up to 20% fuel consumption. The integrated ROPs from each reaction are normalized by the total production or destruction of that species up to 20% fuel decomposition, such that reactions that produce a species are normalized by the total production of the species and reactions that consume a species are normalized by the total consumption of that species. The percentages in Fig. 10 therefore represent the percent of the given reactant that is consumed to form the given product by all reactions that can form a particular product. Species such as hydroperoxyalkyl radicals (QOOH), alkyl hydroperoxides (ROOH), and methylcyclohexenes (MCH-ene) are shown as lumped on the path diagram; however, these species are un-lumped in the mechanism and presented as a lumped sum for simplicity in this diagram. Note that not all of the pathways present in the mechanism for each species are presented in Fig. 10, again for simplicity; the pathways that are shown in Fig. 8 typically account for more than 95% of the consumption of each species.
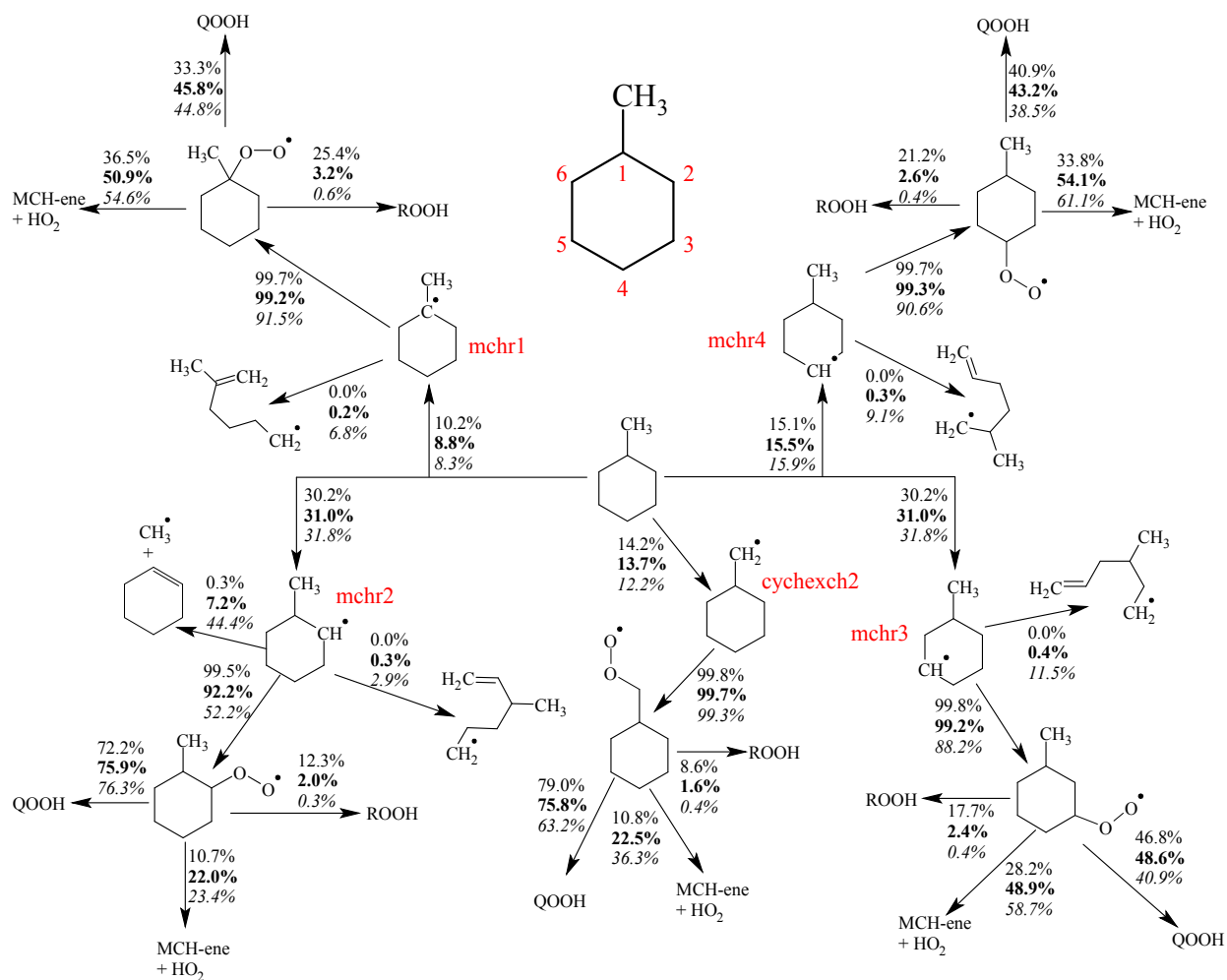
9

Figure 8: Path analysis of MCH combustion. Initial conditions are 25.5 bar and Mix #1 ($\phi = 1.0$) and 700 K (plain text), 800 K (bold text), 900 K (italic text). Note that not all possible reaction pathways are shown for each species.

The first step of fuel breakdown occurs by H-atom abstraction at these pressure and temperature conditions. None of the fuel is directly decomposed by unimolecular reactions. Each of the seven possible radicals are formed in comparable quantities; however, due to the symmetry of MCH, sites 2 and 3 are equivalent to sites 6 and 5, respectively, so mchr2 and mchr3 have close to double the production rate compared to the other radicals. It is interesting to note that the production of mchr2, mchr3, and mchr4 increase as the initial temperature increases and the production of mchr1 and cychexch2 decrease to compensate. However, the change is small, no more than 2 percentage points for each radical.

The most important second step is oxygen addition (i.e. formation of ROO) at all of the initial temperatures in this analysis. The importance of this reaction diminishes for each radical as the initial temperature increases due to the increasing importance of β-scission reactions. At 700 K, less than 0.05% of each of the fuel radicals is consumed via β-scission. Between 800 and 900 K, the percentages of mchr1, mchr2, mchr3, and mchr4 that are decomposed via β-scission increase by several thousand percent each; nevertheless, the absolute change is small and the consumption of these radicals still occurs mostly by oxygen addition. The mchr1, mchr3, and mchr4 radicals undergo scission of the cyclohexyl ring, whereas mchr2 primarily scissions at the methyl-cyclohexyl bond. This beta scission of mchr2 competes significantly with its consumption by O_2 at 900 K. Furthermore, the increasing importance of the ring opening reactions from 800 K to 900 K means that chain propagation pathways (instead of effective chain termination pathways forming methylcyclohexene and hydroperoxyl) are available, increasing the reactivity. Finally, even at the elevated initial temperature of 900 K, cychexch2 does not undergo significant ring opening. Instead, it will scission an H atom from site 1 or steal an oxygen atom from hydroperoxyl to form an alkoxy radical (RO) when it does not undergo oxygen addition (these pathways each only consume about 0.3% of cychexch2 and hence are not shown in Fig. 8).

Returning to the low temperature pathways, there are four important classes of reactions that consume the ROO radicals in the current mechanism. These classes are: C1) internal H-atom transfer (isomerization) to form QOOH; C2) direct elimination of hydroperoxyl and methylcyclohexene;

C3) H-abstraction by ROO from either the fuel or hydroperoxyl to form ROOH; and, C4) reactions among the ROO radicals. Class C4 consumes less than 5% of each of the ROO radicals at 700 K and less than 0.1% for the other temperatures and this class is therefore not shown on the path diagram in Fig. 8. Of the other three classes, C1 (formation of QOOH) is the predominant pathway in the low temperature ignition process. Nevertheless, the direct elimination of methylcyclohexene and hydroperoxyl and the formation of ROOH are important at low temperatures as well.

For all of the temperatures considered here, a majority of the ROOH is formed by reactions of ROO with hydroperoxyl to give ROOH and an oxygen molecule. At the initial temperature of 700 K, approximately 15% of the fuel reacts to form ROOH, indicating its importance in low-temperature MCH combustion. The primary route of ROOH formation in this mechanism (H-abstraction from hydroperoxyl by ROO) has not been well studied at combustion relevant temperatures [15] and is therefore a good candidate for further investigation given its importance in the model for MCH combustion.

As the temperature increases, the formation of ROOH becomes substantially less important while the direct HO_2 elimination reaction becomes more important. The increase in production of methylcyclohexene and hydroperoxyl plays a role in the NTC region of ignition delay because this is effectively a chain terminating channel until the temperature increases enough that the sequence $MCH+HO_2=R+H_2O_2$; $H_2O_2(+M)=2OH(+M)$ becomes important and drives the overall ignition.

Interestingly, for most of the ROO radicals, the change in the fraction of ROO consumed to form QOOH is non-monotonic as temperature increases. That is, for mch1oo, mch3oo, and mch4oo the production of QOOH increases in going from 700 K to 800 K, then decreases going from 800 K to 900 K due to the increasing importance of the HO2 elimination channel (due to nuances in the various reaction paths, mch2oo and chxch2oo do not follow this trend). Furthermore, the branching ratios in the decomposition of the QOOH species change as the temperature is increased (not shown in Fig. 8). At the lowest temperature (700 K), the formation of hydroperoxyalkylperoxy radicals (OOQOOH) is favored, leading to low-temperature chain branching and the two-stage ignition phenomenon. However, at 800 K and 900 K, the QOOH tends to decompose into a heptenone and

12

a hydroxyl radical, or one of three epoxide species. In the current model, both heptenone and the three epoxide species are represented by lumped heptenone and epoxide species; however, due to the apparent importance of these species in the intermediate temperature decomposition of MCH, further investigation of their pathways is warranted.

5.2 Sensitivity Analysis

Our second type of analysis is a brute force, one-at-a-time sensitivity analysis. In this work, the sensitivity of the ignition delay to the reaction rates is considered. Due to the size of the mechanism, only the reactions of the fuel and the fuel radicals up to the OOQOOH species are considered. This approach is justified because many of the reactions of the C0-C4 base mechanism are known to be important to the ignition process (e.g., $H_2O_2(+M)=2OH(+M)$), but we are more interested in the effect of updates to the fuel specific sub-mechanism. The sensitivity index is defined in Eq. (1),

$$S_i = \frac{\ln\left(\tau_{i,2}/\tau_{i,1}\right)}{\ln\left(k_{i,2}/k_{i,1}\right)} \tag{1}$$

where τ is the ignition delay time, either first stage or overall, k is the reaction rate, and subscript i indicates the reaction number. The numbered subscripts in Eq. (1) indicate the type of modification that has been made to the rate of reaction i when computing the ignition delay, as discussed in the following.

The reaction rates are modified by multiplying and dividing the pre-exponential constant by a factor f. Thus, the forward and reverse rates are simultaneously modified. Special care is taken to properly modify reaction rates with pressure dependence and explicit reverse parameters. Each rate is modified sequentially and the ignition delay is computed; the pre-exponential constant is reset to its nominal value before modifying the next reaction. Finally, the nominal ignition delay with no rate modification is computed. Thus, each set of reactor input conditions requires $2N + 1$ model evaluations, where N is the number of reactions considered in the sensitivity analysis and N may be less than or equal to the total number of reactions.

The $2N + 1$ model evaluations result in $4N + 2$ ignition delays if two-stage ignition is present and $2N + 1$ ignition delays otherwise. These ignition delays are used to compute the sensitivity indices according to Eq. (1). In the case of bidirectional sensitivity indices, the subscript 2 in Eq. (1) is associated with multiplication by f and the subscript 1 is associated with division by f, resulting in $2N$ sensitivity indices if two-stage ignition is present and N indices otherwise. In the case of unidirectional sensitivity indices, the subscript 2 is associated with either multiplication or division by f and the subscript 1 is associated with the nominal ignition delay, $\tau_{i,1} = \tau_1$. For unidirectional sensitivity indices, $4N$ indices are obtained if two-stage ignition is present and $2N$ are obtained otherwise.

In this work, the bidirectional sensitivity is used with $f = 10$. For all of the reactions considered here, multiplying and dividing a given rate had opposite effects on the ignition delay. Thus, if the ignition delay increased (relative to the nominal case) when the rate of a certain reaction was multiplied, the ignition delay decreased (relative to the nominal case) when the rate of the same reaction was divided and vice versa. Since $k_{i,2}$ is greater than $k_{i,1}$ by definition, the sensitivity index S_i will be positive if $\tau_{i,2} > \tau_{i,1}$ (i.e. increasing the rate increases the ignition delay) and negative if $\tau_{i,2} < \tau_{i,1}$ (i.e. increasing the rate decreases the ignition delay). The sensitivity analysis is run at the same conditions of the path analysis: CONV simulation, initial temperatures of 700 K, 800 K, and 900 K, initial pressure of 25.5 bar, and Mix #1. As with the path analysis, similar results are obtained for other pressures and mixtures.

Figure 9 shows the sensitivity indices for the five reactions (among all the reactions considered in the present sensitivity analysis) to which the overall ignition delay is most sensitive for each temperature studied (700 K, 800 K, and 900 K). For the results at 700 K and 800 K, the bidirectional sensitivity of the first stage ignition delay to the same reactions is also shown, except for two reactions at 800 K for which the unidirectional sensitivity is plotted. The reasons for this will be discussed in due course. It should be noted that the sensitivity indices of the first stage ignition delay have a slightly different ranking than the indices of the overall ignition delay. Therefore, the rank of the first stage sensitivity index of the reactions shown is given in parentheses next to the

bar. At 700 K, the sensitivity of the overall ignition delay is in red and the sensitivity of the first stage ignition delay is in blue; at 800 K, the sensitivity of the overall ignition delay is in grey and the sensitivity of the first stage ignition delay is in green. The most sensitive reaction affecting the first stage ignition delay at 800 K is found to be MCH+OH=mchr3+H2O, although it is not listed in Fig. 9. At 900 K, there is no first stage ignition, and thus no sensitivity of the first stage ignition delay.

Under the pressure/stoichiometry conditions of the present simulations, 800 K is approximately the highest initial temperature at which distinct two-stage ignition (i.e. two inflection points in the temperature or pressure trace) is found for MCH with the current mechanism. As such, several reactions affect the ignition strongly enough to eliminate the first inflection point. These reactions are given in Table 2 for either multiplication or division of the rate by the factor f=10. The naming convention of the species listed in Table 2 can be found in Fig. 8, Fig. 10, and **??**. Two reactions shown in Table 2 also appear in Fig. 9, namely (R1) mch2oo=mch2ene+ho2 and (R2) mch2qx+o2=mch2qxqj. For these reactions at 800 K, the unidirectional sensitivity index is shown in Fig. 11, where $\tau_{i,2}$ in Eq. (1) is found by division of the rate for $i = R1$ and by multiplication of the rate for $i = R2$.

The role of the ROO=methylcyclohexene+HO2 reactions in the left column of Table 2 in eliminating the first stage of ignition is clear -- this set of reactions diverts ROO radicals from entering the low-temperature chain branching pathway via QOOH that leads to the two-stage ignition. Similarly, in the right column, decreasing the rate of the reaction of oxygen with QOOH to form OOQOOH reduces the rate of chain branching that leads to two-stage ignition. Concerning the reactions of the fuel with OH in the left column of Table 2, increasing these rates increases the formation of fuel radicals that are less reactive at low temperature than the cychexch2 and mchr2 radical. For example, the mchr2 radical adds to O_2 and forms a peroxy radical (mch2oo) that has a fast RO2 isomerization path to QOOH involving the abstraction of an H atom from the methyl group. This ROO isomerization is the path calculated and discussed in Section 4.1 of [**Weber2014**]. QOOH subsequently adds to O_2 and leads to chain branching. The high reactivity of cychexch2

Table 2: Reactions that eliminate the first inflection point for a nominal case with two-stage ignition.

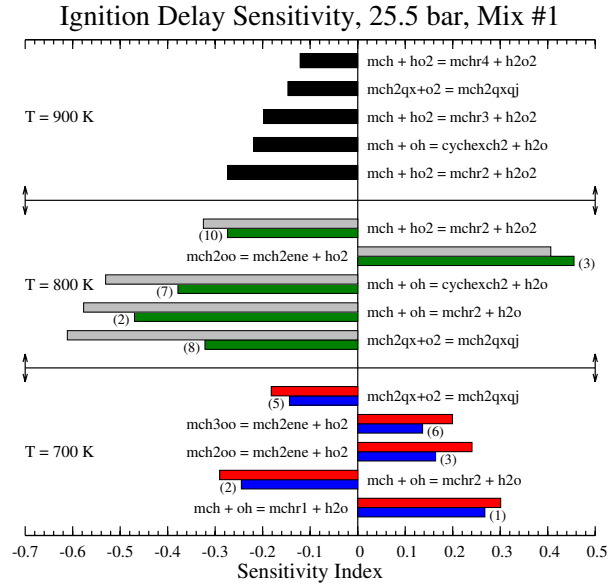| Multiplication	Division
mch2oo = mch2ene + ho2	mch2qx + o2 = mch2qxqj
mch3oo = mch2ene + ho2	
mch3oo = mch3ene + ho2	
mch + oh = mchr1 + h2o	
mch + oh = mchr4 + h2o	
mch + oh = mchr3 + h2o	

Figure 9: Sensitivity of the ignition delay to various reaction rates for Mix #1 ($\phi = 1.0$), 25.5 bar and three temperatures (700 K, 800 K, and 900 K). At 700 K, the sensitivity of the overall ignition delay is in red and the sensitivity of the first stage ignition delay is in blue. At 800 K, the sensitivity of the overall ignition delay is in grey and the sensitivity of the first stage ignition delay is in green. At 900 K, the sensitivity of the overall ignition delay is in black. Numbers in parentheses represent the ranking of the first stage sensitivity indices.

and mchr2 at low temperature is reflected by the high percentages at 800 K (>70%) leading to QOOH from cychexch2oo and mch2oo in Fig. 8.
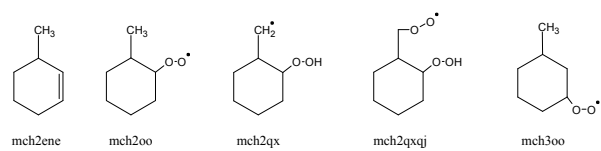
Figure 10: Species mentioned in Fig. 9 or Table 2 and not included in Fig. 8.